

# Unsupervised Out-of-Distribution Detection Using Kernel Density Estimation

Ertunc Erdil\*, Krishna Chaitanya, Neerav Karani, Ender Konukoglu

Computer Vision Lab, ETH Zurich  
Sternwartstrasse 7, Zurich 8092, Switzerland  
\*ertunc.erdil@vision.ee.ethz.ch

## Abstract

Deep neural networks (DNNs) achieve substantial advancement to the state-of-the-art in many computer vision tasks. However, accuracy of DNNs may drop drastically when test data come from a different distribution than training data. Detecting out-of-distribution (OOD) samples before performing downstream analysis on the predictions of a DNN thus arises as a crucial problem for critical applications, such as medical diagnosis and autonomous driving. The majority of the existing methods focus on OOD detection in the classification problem. In this paper, we propose an unsupervised OOD detection method using kernel density estimation (KDE), which is a non-parametric method for estimating probability density functions (pdfs). Specifically, we estimate the pdfs of features for each channel of the network, by performing KDE on the in-distribution (InD) dataset. At test time, the pdfs are evaluated on the test data to obtain a confidence score for each channel, which is expected to be higher for InD and lower for OOD samples. These scores are combined into a final score using logistic regression. Crucially, the proposed method does not require class labels nor information on the output of a network. Thus, it can be used for networks both for classification and non-classification problems. Furthermore, the use of KDE eliminates the need for making a parametric assumption (e.g. Gaussian) about feature densities. We performed experiments on 2 different classification networks trained on CIFAR-10 and CIFAR-100, and 2 different non-classification networks (segmentation and detection) trained on COCO dataset. The proposed method achieved detection accuracy on-par with the state-of-the-art for classification networks, even surpassing them with high margins in the majority of the tests. Additionally, the proposed method substantially outperformed the compared alternatives for segmentation and detection networks in all the tests, thus exhibiting a larger scope of applications than existing methods.

## 1 Introduction

Deep neural networks (DNNs) can perform predictions on test images with very high accuracy when the training and testing data come from the same distribution. However, the prediction accuracy decreases rapidly if the test image is sampled from a different distribution than the training data. Furthermore, DNNs make predictions in such cases with

very high confidence (Guo et al. 2017). This creates a big obstacle when deploying DNNs for real applications, especially for the ones with a low tolerance for error such as autonomous driving and medical diagnosis. Therefore, it is crucial to improve the robustness of DNN-based methods and prevent them from making big mistakes (Amodei et al. 2016). Automatic detection of OOD samples can play a key role to this end. Despite the success of existing OOD detection methods, most of them operate on DNNs designed for classification tasks. However, OOD detection is important not only for classification but also for non-classification tasks, such as segmentation and detection.

## Related Work

We describe the OOD detection methods in the literature by grouping them in three categories.

**Softmax probabilities for OOD detection:** Hendrycks et al. (2017) propose a baseline OOD detection method by exploiting probabilities from the softmax outputs of a classification DNN. Another method, *ODIN* (Liang, Li, and Srikant 2017), extends the baseline by applying an adversarial perturbation to the input image (referred to as input pre-processing). Additionally, while computing the OOD confidence score, so-called temperature scaling is applied by dividing the input of the softmax by a scaling parameter. Both of these steps are designed to increase the difference between the scores of InD and OOD samples. Hsu et al. (2020) further extend ODIN by proposing a method called Generalized ODIN (*G-ODIN*), where a random variable is introduced to indicate whether each sample is InD or OOD. The penultimate layer of a DNN is decomposed into two branches to model the conditional distribution of this new variable and its joint distribution with the class label given the input image. The final class prediction probabilities are obtained by dividing the output of the joint distribution by the output of the conditional distribution. Confidence score for OOD detection is obtained by taking the output of one of the two branches after applying input pre-processing.

**Training strategies for OOD detection:** DeVries and Taylor (2018) introduce a confidence estimation network branch, and use the confidence estimates obtained from this branch in order to train the softmax probabilities of the classification network. Lee et al. (2018a) present a training

method for classifier networks so that they become less confident for OOD examples. They introduce two loss terms in addition to the cross-entropy. The first one encourages the network to become less confident for the OOD examples whereas the second one generates the most optimal OOD examples for the first one. Vyas et al. (2018) use an ensemble of classifiers for OOD detection, where each classifier is trained by leaving-out a different class from the InD training set. OOD detection is then performed based on the ensemble of softmax probabilities of each classifier, after applying temperature scaling and input pre-processing as in ODIN.

**Density estimation for OOD detection:** Lee et al. (2018b) propose a method named as *Mahalanobis*, which assumes that the class conditional pdfs of the features at intermediate layers of a DNN can be represented by a Gaussian density for InD samples. The parameters of each class conditional Gaussian are estimated by computing the empirical mean and co-variance using InD training samples and the corresponding class labels. At test time, input pre-processing is applied before evaluating the estimated densities to obtain a confidence score, which is expected to be higher for InD samples and lower for OOD samples.

Among all the aforementioned methods, G-ODIN and Mahalanobis demonstrate state-of-the-art results on benchmark classification datasets. However, all these methods are designed for OOD detection for classification tasks. Extending them to other tasks is non-trivial, as they exploit class information either directly or via the class prediction probabilities of the DNN. Addressing this limitation, Hendryks et al. (2019) propose an OOD detection method that trains an auxiliary rotation network on the InD dataset and computes a confidence score for a test image as the maximum of the softmax activation. The scores are expected to be higher for InD images and lower for OOD. As this method operates on an auxiliary self-supervised network that is detached from the main network, it can be applied to non-classification tasks as well.

## Motivation

The Mahalanobis method (Lee et al. 2018b) achieves state-of-the-art results on classification DNNs for a number of computer vision benchmark datasets. Despite its success, there are some weaknesses that limit its application on tasks other than classification and may lead to diminished accuracy: 1) the method estimates class conditional feature densities at different layers of a network. However, feature vectors at the intermediate layers are usually very high dimensional, thus making density estimation error-prone due to the *curse-of-dimensionality*. Although, they take channel-wise mean to reduce the dimensionality from  $C \times H \times W$  to  $C \times 1$  before density estimation, the resulting feature vector is still high dimensional, 2) estimating class conditional densities of image features requires class label information of images which may not be available for the tasks other than classification, 3) the Gaussian assumption about the class conditional densities in the feature space may not necessarily hold for all datasets, which can diminish the OOD detection performance. This motivates us to develop a new OOD detec-

tion method that addresses the above-mentioned weaknesses to achieve a better OOD detection performance in both classification and non-classification networks.

## Contribution

In this paper, we propose an unsupervised OOD detection method using kernel density estimation (KDE). The proposed method extends Lee et al. (2018b) and addresses its weaknesses by 1) estimating a separate 1-dimensional density for each channel at different layers instead of estimating a single density for the entire layer in  $C$ -dimensional space, 2) eliminating the need for class labels by estimating the marginal density of features instead of class conditional feature densities, 3) performing non-parametric KDE instead of making a parametric density assumption (e.g. Gaussian) about the underlying densities. These design choices enable the proposed method to achieve a more accurate density estimation in a non-parametric way using KDE in 1-dimensional space and lead to improved OOD detection accuracy. Moreover, eliminating the need for class labels makes the method applicable to non-classification networks, where class labels are not available.

Concretely, the proposed method consists of the following steps: First, we estimate the feature densities for each channel of a DNN via KDE, using training images from the InD dataset. Secondly, analogous to Lee et al. (2018b), we train a logistic classifier for OOD detection to combine the confidence scores of all channels into a single confidence score. In order to train this classifier, we use images from the available training dataset as InD samples and adversarially perturb them in order to get OOD samples. Thus, the proposed method does not require example OOD samples during training time. Finally, for each test image, we evaluate the KDE confidence scores for each layer, and combine them using the trained logistic classifier to obtain a final confidence score that indicates the probability of the test image being InD.

We perform experiments on 2 different classification networks trained on CIFAR-10 and CIFAR-100 datasets (Krizhevsky, Hinton et al. 2009) by using 6 datasets as OOD. We compare with 4 OOD detection methods: Baseline (Hendrycks and Gimpel 2017), ODIN (Liang, Li, and Srikant 2017), Mahalanobis (Lee et al. 2018b), and G-ODIN (Hsu et al. 2020), which are all primarily designed for OOD detection in classification networks. For both networks, the proposed method achieves state-of-the-art performance for most OOD datasets, according to various evaluation metrics.

Furthermore, we perform experiments on two non-classification tasks: segmentation and detection. For both these tasks, we use the COCO dataset (Lin et al. 2014) for training, by using appropriate labelling according to the task. We use 4 datasets as OOD and compare the proposed method with a modified version of Mahalanobis (Lee et al. 2018b) and a recent OOD detection work (Hendrycks et al. 2019) that also does not require image labels. In both of our non-classification experiments, we achieve the state-of-the-art results on all OOD datasets.

## 2 Method

Let us assume that we have a set of training images  $X_{tr} = \{x_1, x_2, \dots, x_M\} \sim P_{in}$  and corresponding labels  $y_{tr} = \{y_1, y_2, \dots, y_M\}$ , where  $P_{in}$  denotes the InD. Let us also assume that we have a DNN,  $f$ , trained using  $(X_{tr}, y_{tr})$ .  $f$  is more likely to perform good predictions on a test image  $x_{test}$  if  $x_{test} \sim P_{in}$  and incorrect predictions if  $x_{test} \sim P_{out}$ , where  $P_{out} \neq P_{in}$ . In this section, we introduce the proposed KDE-based approach that identifies test images sampled from  $P_{out}$ . The application of the proposed model at test time is summarized in Algorithm 1.

---

### Algorithm 1: The proposed method

---

**Input:** Test Image:  $x$   
 Random subset of training images:  
 $\hat{X}_{tr} = \{x_{u_1}, x_{u_2}, \dots, x_{u_N}\}$   
 Weights of logistic regression classifier:  $\alpha_{lc}$   
 Set of kernel sizes:  $\sigma$   
**Output:** Confidence score of  $x$ :  $\mathcal{M}_x$ .

```

foreach  $l \in L$  do
  for  $c \leftarrow 1$  to  $C_l$  do
    Perform KDE at channel  $c$  of the feature map
    at layer  $l$ :
     $\hat{p}_{lc}(x) = \frac{1}{N} \sum_{i=1}^N \mathcal{K}(f_{lc}(x) - f_{lc}(x_{u_i}); \sigma_{lc})$ 
  end
end
return  $\mathcal{M}_x = \sum_{l=1}^L \sum_{c=1}^{C_l} \alpha_{lc} \hat{p}_{lc}(x)$ 

```

---

### Computing the confidence scores

Let us assume that the DNN,  $f$ , consists of  $L$  layers.  $f$  outputs a  $C_l \times H \times W$  feature map  $f_l(x)$  for an input image  $x$  at layer  $l$ , where  $C_l$ ,  $H$ , and  $W$  is the number of channels, height, and width of the feature map, respectively. In DNNs, feature maps are typically very high-dimensional and estimating their probability density functions is non-trivial due to the curse of dimensionality (Scott 2015). In order to tackle this problem, we take the channel-wise mean of the feature vector and reduce the dimensionality to  $C_l \times 1$ , as suggested by Lee et al. (2018b). We denote the resulting  $C_l$ -dimensional feature vector by  $f'_{lc}(x)$ . Even after this reduction in dimensionality, performing density estimation in the  $C_l$ -dimensional space may still be error-prone as the number of channels,  $C_l$ , in modern DNN architectures can be very large. Therefore, in the proposed method, we estimate a 1-dimensional probability density function for each channel using KDE

$$p_{lc}(x) \approx \hat{p}_{lc}(x) = \frac{1}{M} \sum_{i=1}^M \mathcal{K}(f'_{lc}(x) - f'_{lc}(x_i); \sigma_{lc}) \quad (1)$$

where  $p_{lc}$  is the true probability density function,  $\hat{p}_{lc}$  is its estimation using KDE,  $f'_{lc}(x)$  is the mean activation value of the channel  $c$  in the feature map at layer  $l$ , and  $\mathcal{K}(\cdot; \sigma_{lc})$  is the KDE kernel with size  $\sigma_{lc}$ . We choose  $\mathcal{K}$  as a 1D Gaussian kernel with zero mean. The procedure used to set the kernel size  $\sigma_{lc}$  is described in detail later in this section.

Note that, in order to estimate  $p_{lc}$  in Eq. (1), we need to store all the InD training images in  $X_{tr}$ . In real-world applications where  $M$  is very large, storing the entire  $X_{tr}$  may not be feasible and the summation over  $M$  images in Eq. (1) can take very long. Improving the computational and memory efficiency of KDE-based methods are possible by defining an unbiased estimator (Erdil et al. 2019). We achieve this by selecting a random subset of  $X_{tr}$  such that

$$\hat{X}_{tr} = \{x_{u_1}, x_{u_2}, \dots, x_{u_N}\} \subset X_{tr}$$

where  $\{u_1, u_2, \dots, u_N\} \subset \{1, 2, \dots, M\}$  is a random subset of indices generated by sampling from a Uniform density,  $\mathcal{U}(1, M)$ , without replacement and  $N \ll M$ . Using the random subset, we replace the summation in Eq. (1) with the computationally more efficient unbiased estimator

$$p_{lc}(x) \approx \hat{p}_{lc}(x) = \frac{1}{N} \sum_{i=1}^N \mathcal{K}(f'_{lc}(x) - f'_{lc}(x_{u_i}); \sigma_{lc}). \quad (2)$$

Once we obtain the confidence scores  $\hat{p}_{lc}(x)$  for each channel  $c$  at layer  $l$  using Eq. (2), we compute the final confidence score as

$$\mathcal{M}_x = \sum_{l=1}^L \sum_{c=1}^{C_l} \alpha_{lc} \hat{p}_{lc}(x) \quad (3)$$

where  $\alpha_{lc}$  are the parameters of a logistic regression classifier which we describe in the following subsection.

### Learning logistic regression parameters $\alpha_{lc}$

The proposed method computes the final confidence score  $\mathcal{M}_x$  from the scores predicted at each layer  $l$  and channel  $c$  using a logistic regression classifier with parameters  $\alpha_{lc}$  (see Eq. (3)). Training the classifier to learn  $\alpha_{lc}$  requires having access to both InD and OOD images. Although the InD images,  $X_{tr}$ , are already available, it is difficult to capture all possible images not included in  $P_{in}$ . Lee et al. (2018b) propose using adversarial examples as samples from  $P_{out}$  to train the logistic regression classifier. We follow the same approach in the proposed method. Once the OOD samples are obtained by applying adversarial perturbation to the images in  $X_{tr}$ , the logistic regression classifier is trained by using the confidence scores  $\hat{p}_{lc}$  as inputs and the output labels are provided as positive for InD images and negative for the OOD ones.

### Determining size of KDE kernel

Kernel size,  $\sigma$ , is a crucial parameter of KDE since it significantly effects the shape of the estimated density. Setting  $\sigma$  to a large value leads to very smooth pdfs, reducing the likelihood of the observed samples as well as other samples from the same distribution. On the other hand, setting  $\sigma$  to a very small value leads to very peaky distributions only attributing high probability to observed samples, and assigning very low probability to unobserved samples even from the same distribution. Therefore, finding an optimal  $\sigma$  value is quite important in order to capture the underlying pdf of the data (Scott 2015).

In the proposed method, as given in Eq. (2), we use a different  $\sigma_{lc}$  for each channel  $c$  and layer  $l$ . To compute  $\sigma_{lc}$ , we use the  $k$ -nearest neighbor method ( $k$ NN) (Silverman 1986). Specifically, we compute the distance between  $f'_{lc}(x_{u_i})$  and  $f_{lc}(x_{u_j})$  for all  $i, j \in [1, N]$ ,  $i \neq j$  and set  $\sigma_{lc}$  as the  $k^{th}$  smallest value. We denote the set of all  $\sigma_{lc}$  values by  $\sigma$ .

A parameter of the  $k$ NN method is the  $k$  itself. In the proposed method, we automatically select the most appropriate  $k$  value from a set of candidate values denoted by  $\mathbf{k}$ . To achieve this, we split a validation set  $X_{val}$  from  $X_{tr}$  by taking the samples that are not used in KDE. Then, we apply adversarial perturbation to the images in  $X_{val}$  and obtain  $X_{val}^{adv}$  as OOD examples. We select the  $k \in \mathbf{k}$  that maximizes the difference between the InD and OOD datasets.

$$k_{lc} = \arg \max_{k \in \mathbf{k}} \sum_{x \in X_{val}} \hat{p}_{lc}(x) - \sum_{x' \in X_{val}^{adv}} \hat{p}_{lc}(x') \quad (4)$$

where  $k_{lc}$  indicates the optimum  $k$  value in layer  $l$ . In our experiments, we choose  $k_l$  from the candidate set  $\mathbf{k} = \{1, 2, 5, 10, 15, 20, 50\}$  using the described method.

### 3 Experimental results

#### Datasets and network architectures

We evaluate the performance of the proposed approach on both classification and non-classification networks and compare them with the state-of-the-art OOD detection methods. The proposed method is implemented in PyTorch and we run all experiments on a Nvidia GeForce Titan X GPU with 12GB memory. In the classification experiments, we train two different networks on CIFAR-10 and CIFAR-100 (Krizhevsky, Hinton et al. 2009) that contain images from 10 and 100 classes, respectively. Both datasets contain 50000 training and 1000 test images where each one is a  $32 \times 32$  color image. We compare the proposed method with the Baseline method of Hendrycks et al. (Hendrycks and Gimpel 2017), ODIN (Liang, Li, and Srikant 2017), Mahalanobis (Lee et al. 2018b), and G-ODIN (Hsu et al. 2020) which are primarily designed for OOD detection in classification networks. We perform OOD detection on the ResNet (He et al. 2016) models trained on CIFAR-10 and CIFAR-100 by Lee et al. (2018b) using all methods<sup>1</sup>.

We use 6 different datasets as OOD<sup>2</sup>: SVHN (Netzer et al. 2011) contains 26032 images of house numbers in Google street-view images. Resized TinyImageNet (Tin-rs) and cropped TinyImageNet (Tin-cr) consist of 10000  $32 \times 32$  RGB test images which are obtained by resizing and cropping a subset of the original ImageNet dataset (Deng et al. 2009), respectively. Resized LSUN (LSUN-rs) and cropped LSUN (LSN-cr) contain 10000 RGB test images with size  $32 \times 32$  and they are obtained by resizing and cropping a subset of the original LSUN dataset (Yu et al. 2015). iSUN is a subset of SUN dataset (Xu et al. 2015) that contains 8925 RGB images resized to  $32 \times 32$ .

<sup>1</sup>Pretrained models are available at [https://github.com/pokaxpoka/deep\\_Mahalanobis\\_detector](https://github.com/pokaxpoka/deep_Mahalanobis_detector)

<sup>2</sup>Tin-rs, Tin-cr, LSUN-rs, LSUN-cr, and iSUN are available at <https://github.com/facebookresearch/odin>

In the non-classification experiments, we use two different networks: one for a segmentation task and the other for a detection task. In the experiments on segmentation network, we use the DeeplabV3 (Chen et al. 2017) architecture that has ResNet (He et al. 2016) backbone pre-trained on COCO dataset (Lin et al. 2014) with the segmentation masks as label. In the experiments with the detection network, we use Faster R-CNN (Ren et al. 2015) pre-trained on the COCO dataset with the object coordinates as the label. Both pre-trained models are available in PyTorch.

COCO dataset contains 118287 annotated training images and 40670 test images. We compare the proposed method with 2 different OOD detection methods: a modified version of Mahalanobis (Lee et al. 2018b) and the self-supervised learning-based (SSL) method proposed in (Hendrycks et al. 2019). Mahalanobis is originally designed for OOD detection in classification networks, and it requires class labels for each image in the InD dataset. To modify Mahalanobis for non-classification networks, we assign the same label to all images. We use the same DeeplabV3 and Faster R-CNN networks to evaluate the modified Mahalanobis. SSL uses a self-supervised rotation network for OOD detection. Since SSL performs OOD detection on a network that is independent from the main network, it can be used for both classification and non-classification networks. To compare with SSL (Hendrycks et al. 2019), we randomly rotate the training images in the COCO dataset and train a neural network that predicts the rotation angle using a ResNet architecture. Then, the confidence scores for OOD detection for a test image are obtained by taking the maximum of the softmax probabilities as proposed in (Hendrycks et al. 2019) for classification networks.

In non-classification experiments, we use 4 different datasets as OOD. Pascal VOC (Everingham et al. 2010) dataset contains 1464 annotated training images and 1449 test images. KITTI (Alhaija et al. 2018) contains 200 test images of street scenes. Berkeley Deep Drive (BDD) (Yu et al. 2020) is another dataset that contains images of street scenes and includes 2000 test images. Finally, Places (Zhou et al. 2017) datasets that we use as OOD contains 328500 test images. We use a random subset of 10000 images of the Places dataset in our experiments for computational purposes.

#### Evaluation methods

We used the same evaluation methods that are commonly used for evaluating OOD detection methods in the literature (Hendrycks and Gimpel 2017). In all methods, we take the InD as the positive class and OOD as the negative class.

**FPR at 95% TPR:** False positive rate (FPR) is measured when the true positive rate (TPR) of 95% is reached at a certain threshold. The false positive rate is calculated as  $FPR = FP / (FP + TN)$  and true positive rate is calculated as  $TPR = TP / (TP + FN)$  where TP, FP, TN, and FN represent true positive, false positive, true negative, and false negative, respectively.

**Detection error:** This metric measures the probability of wrong classification when TPR is 95%. We denote the detection error by  $P_{err}$  and compute as  $P_{err} = 0.5(1 - TPR + FPR)$ .

OOD	FPR at 95% TPR ↓				AUROC ↑				Detection Error ↓																		
	Baseline / ODIN / Mahalanobis / G-ODIN / <b>Proposed</b>																										
SVHN	25.77	/	17.65	/	<b>4.09</b>	/	10.50	/	6.80	89.88	/	95.42	/	<b>99.04</b>	/	97.80	/	97.87	15.38	/	11.32	/	<b>4.54</b>	/	-	/	5.90
TIN-rs	28.37	/	11.24	/	59.55	/	18.60	/	<b>1.91</b>	90.95	/	96.78	/	81.21	/	96.10	/	<b>99.05</b>	16.68	/	8.12	/	32.27	/	-	/	<b>3.45</b>
TIN-cr	24.29	/	<b>7.56</b>	/	33.29	/	18.90	/	72.01	92.33	/	<b>98.07</b>	/	88.82	/	96.00	/	78.88	16.64	/	<b>6.28</b>	/	19.14	/	-	/	38.50
LSUN-rs	28.31	/	10.39	/	29.68	/	9.10	/	<b>1.12</b>	91.05	/	97.06	/	92.94	/	96.0	/	<b>99.62</b>	16.65	/	7.69	/	17.34	/	-	/	<b>3.06</b>
LSUN-cr	16.75	/	<b>4.67</b>	/	14.78	/	12.7	/	79.79	94.35	/	<b>98.71</b>	/	96.38	/	97.2	/	71.63	10.87	/	<b>4.83</b>	/	9.89	/	-	/	42.39
iSUN	28.02	/	12.37	/	30.81	/	11.2	/	<b>2.06</b>	91.01	/	96.03	/	92.64	/	97.6	/	<b>98.93</b>	16.51	/	8.68	/	17.90	/	-	/	<b>3.53</b>

Table 1: Quantitative results on distinguishing test set of CIFAR-10 InD dataset from several OOD datasets. ↑ indicates larger value is better and ↓ indicates lower value is better. *All values are percentages.*

OOD	FPR at 95% TPR ↓				AUROC ↑				Detection Error ↓																		
	Baseline / ODIN / Mahalanobis / G-ODIN / <b>Proposed</b>																										
SVHN	55.73	/	24.76	/	9.00	/	44.90	/	<b>4.87</b>	79.34	/	92.13	/	97.63	/	93.20	/	<b>98.05</b>	30.36	/	14.88	/	7.00	/	-	/	<b>4.93</b>
TIN-rs	58.97	/	26.85	/	24.90	/	23.50	/	<b>6.18</b>	77.07	/	88.32	/	94.63	/	95.9	/	<b>98.18</b>	31.98	/	19.37	/	14.95	/	-	/	<b>5.58</b>
TIN-cr	52.69	/	<b>26.85</b>	/	44.24	/	27.40	/	78.15	82.02	/	92.00	/	91.15	/	<b>95.30</b>	/	75.01	28.84	/	<b>15.92</b>	/	16.04	/	-	/	41.57
LSUN-rs	64.71	/	37.09	/	26.66	/	23.20	/	<b>1.70</b>	75.58	/	87.77	/	93.08	/	96.10	/	<b>99.41</b>	34.85	/	21.04	/	15.83	/	-	/	<b>3.35</b>
LSUN-cr	66.95	/	<b>34.78</b>	/	32.58	/	34.30	/	65.22	77.19	/	88.94	/	92.19	/	<b>93.80</b>	/	81.54	35.97	/	19.89	/	<b>10.95</b>	/	-	/	35.11
iSUN	63.26	/	38.21	/	28.86	/	24.70	/	<b>4.41</b>	75.68	/	86.73	/	93.31	/	95.70	/	<b>98.91</b>	34.13	/	21.06	/	16.93	/	-	/	<b>4.70</b>

Table 2: Quantitative results on distinguishing test set of CIFAR-100 InD dataset from several OOD datasets. ↑ indicates larger value is better and ↓ indicates lower value is better. *All values are percentages.*

**AUROC:** The Area Under the Receiver Operating Characteristic curve (AUROC) is a threshold independent method that measures the area below Receiver Operating Characteristic (ROC) curve (Davis and Goadrich 2006). ROC curve reflects the relationship between TPR and FPR values as the threshold changes. AUROC takes its highest value at 100% when the detection is perfect.

## Results and Analysis

In this section, we present the quantitative results obtained for both the classification and non-classification tasks introduced earlier.

**In the classification experiments,** we compare the proposed method with Baseline, ODIN, Mahalanobis, and G-ODIN. ODIN, Mahalanobis, and G-ODIN have important parameters that significantly affect their performance. These parameters are temperature scaling and input pre-processing magnitude for ODIN and G-ODIN, and only the input pre-processing magnitude for Mahalanobis. We choose these parameters from the list of values given in the original papers by using a validation set that contains InD training and adversarial images for ODIN and Mahalanobis. The best-performing parameters in terms of FPR at 95% TPR are chosen for each InD dataset. The implementation of G-ODIN is not publicly available, but as our experiment settings such as network architecture and OOD datasets are similar to their work (Hsu et al. 2020), we directly use the results from their paper for comparison. Note that the detection error column is missing for G-ODIN in the presented results in Tables 1 and 2 since evaluation with this metric is not available in the original paper. For the proposed method, we set  $N = 5000$  in both classification and segmentation experiments, where  $N$  is the number of images from the InD dataset used for

estimating the densities using KDE (see Sec. 2).

In Table 1, we present the quantitative OOD detection results on a DNN trained on the CIFAR-10 dataset. These results show that the proposed method achieves the best performance, with a significant improvement over the state-of-the-art methods on 3 out of 6 OOD datasets (TIN-rs, LSUN-rs, and iSUN) and the second best results on the SVHN dataset. OOD detection performance of the proposed method diminishes in TIN-cr and LSUN-cr datasets, where ODIN achieves the best performance.

In Table 2, we present the quantitative OOD detection results on a DNN trained on CIFAR-100 dataset. In this experiment, the proposed KDE-based method achieves improvement with a significant margin over the state-of-the-art methods on 4 out of 6 OOD datasets (SVHN, TIN-rs, LSUN-rs, and iSUN). Analogous to the CIFAR-10 experiments, we observe diminished OOD detection performance on the cropped datasets (TIN-rs and LSUN-rs) in the CIFAR-100 experiments as well.

**Analysis of OOD detection in classification task:** We perform analysis to interpret the results for each OOD dataset. The logistic regression classifier is trained to distinguish the scores  $\hat{p}_{lc}(x)$  of InD images from the OOD ones. Even though the OOD space is potentially too large to capture with such a small sample set, we observe that overall trends of OOD detection performance of channels are similar for most OOD datasets, including the adversarial images. In Fig. 1, we visualize these trends by plotting AUROC values obtained at each channel using the channel-wise confidence scores  $\hat{p}_{lc}$  for SVHN, TIN-rs, TIN-cr, LSUN-rs, LSUN-cr, iSUN datasets, and adversarial images when the InD is CIFAR-10. Having similar trends between adversarial images and the other OOD datasets indicates that a logistic re-

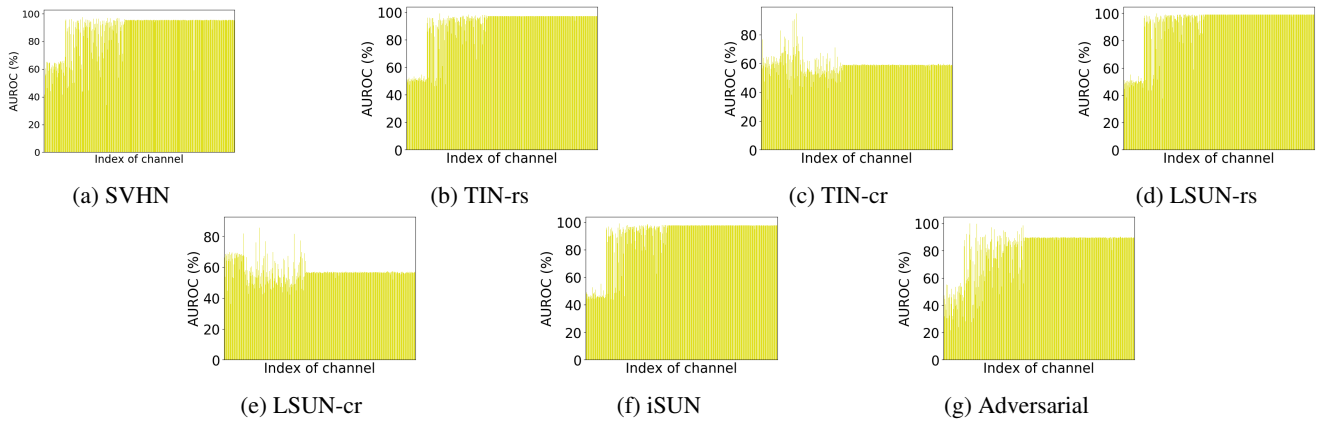


Figure 1: Trends of channel-wise OOD detection performance evaluated with AUROC for different OOD datasets when the InD dataset is CIFAR-10. The plots show that the AUROC trend of adversarial images is similar to most of the OOD datasets, indicating that the logistic regression classifier trained using adversarial images can generalize to most of the OOD datasets.

OOD	FPR at 95% TPR ↓		AUROC ↑		Detection Error ↓				
	SSL	Mahalanobis	Proposed	SSL	Mahalanobis	Proposed			
Pascal VOC	95.42	96.05	<b>13.92</b>	50.87	52.99	<b>97.27</b>	50.21	50.52	<b>9.48</b>
KITTI	88.81	97.91	<b>42.65</b>	58.29	21.55	<b>94.35</b>	46.90	51.35	<b>23.82</b>
BDD	94.07	89.53	<b>38.58</b>	51.95	51.50	<b>95.71</b>	49.53	47.26	<b>21.79</b>
Places	94.67	96.23	<b>12.46</b>	50.68	47.81	<b>97.55</b>	49.83	50.61	<b>8.73</b>

Table 3: Quantitative results on distinguishing test set of COCO InD dataset from several OOD datasets in the segmentation network. ↑ indicates larger value is better and ↓ indicates lower value is better. *All values are percentages.*

gression classifier trained using  $X_{tr}$  (positive class) and its adversarial versions (negative class) can generalize to other OOD datasets. It can be seen that the AUROC trends for SVHN, TIN-rs, LSUN-rs, and iSUN are similar to the adversarial images, where AUROC results are low in the earlier channels and high in the later ones. The similarity between the trends explains the high OOD detection performance of the proposed method in these datasets. On the contrary, AUROC results are higher in the earlier channels for the TIN-cr and LSUN-cr datasets and the trends are not aligned with the adversarial images. The difference between the trends negatively affects the generalization performance of the logistic regression classifier to these datasets and results in diminished OOD detection performance. The reason of having higher AUROC scores in TIN-cr and LSUN-cr datasets could be that these are cropped images and do not contain many low-level features such as edges and corners unlike the InD images - instead, they mostly consist of smooth regions. Since the earlier layers of the networks extract such features, higher OOD detection performances are obtained in the earlier channels.

**In the segmentation experiments,** we compare the proposed method with two methods (Mahalanobis and SSL) that can operate on non-classification networks for OOD detection. The quantitative results obtained on 4 OOD datasets with 3 evaluation methods are shown in Table 3. The results demonstrate that the proposed method achieves significant improvement over the existing methods. SSL uses output

probabilities of a self-supervised auxiliary rotation network for OOD detection. DNNs may not learn dataset-specific features to perform well on a rotation task and can generalize to other OOD datasets. This is the case with the rotation network in SSL because the accuracy of the rotation network is  $\sim 75\%$  for both the InD test set and the OOD datasets, which makes it hard to distinguish OOD datasets by looking at the softmax outputs. In non-classification networks, the image-level class label information is usually not available. Therefore, in this experiment, the Mahalanobis method models feature densities at different layers using a single Gaussian per layer by assuming all images to have the same label. The lower OOD detection accuracy with this method indicates that the Gaussian assumption may not be optimal to model the feature densities. Instead, the non-parametric KDE method appears to be better suited for estimating the channel-wise feature densities and achieves quite a substantial improvement over other methods.

**In the detection experiments,** we compare the proposed method with Mahalanobis and SSL, and present the quantitative results in Table 4. As mentioned before, SSL operates on an auxiliary self-supervised network, and its performance is not affected by the architecture of the main network. This means that the result of the SSL remains the same for both segmentation and detection experiments on the COCO dataset. Therefore, we do not re-write the results of SSL in Table 4. Similar to the segmentation network experiments, the proposed method performs better than both

Mahalanobis and SSL on the detection networks. These results demonstrate the potential of the proposed method on non-classification networks.

OOD	FPR at 95% TPR ↓		AUROC ↑
	Mahalanobis / <b>Proposed</b>		
Pascal VOC	94.29 / <b>5.24</b>	48.49 / <b>99.00</b>	
KITTI	98.74 / <b>4.61</b>	14.58 / <b>99.06</b>	
BDD	91.27 / <b>8.78</b>	46.52 / <b>98.35</b>	
Places	96.23 / <b>1.84</b>	46.35 / <b>99.07</b>	

Table 4: Quantitative results on distinguishing test set of COCO InD dataset from several OOD datasets in the detection network. Note that we do not include the SSL results to this table since SSL operates on an auxiliary network and its performance on the same dataset does not change for different architectures. Therefore, it produces the same results for both segmentation and detection experiments on COCO which are already given in Table 3.

	Layer-wise		Channel-wise	
	Gaussian (Mahalanobis)	KDE	Gaussian	KDE (Proposed)
SVHN	9.00	24.09	6.09	<b>4.87</b>
TIN-rs	24.90	34.08	10.60	<b>6.18</b>
LSUN-rs	26.66	28.47	<b>1.45</b>	1.70
iSUN	28.86	33.49	4.99	<b>4.41</b>

Table 5: Comparison between different combinations of density estimation methods (Gaussian and KDE) with feature spaces (layer-wise and channel-wise) in terms of FPR at 95% TPR in CIFAR-100 dataset.

**Analysis on the choice of channel-wise v/s layer-wise features and KDE v/s parametric density estimation:** In the proposed approach, we perform KDE on each channel to perform OOD detection. In this section, we present the results of the analysis to understand which component of the proposed method is more useful for OOD detection: (a) feature selection (layer-wise v/s channel-wise features) or (b) density estimation method used (KDE v/s Gaussian). We perform this analysis by comparing the results obtained by using different combinations of feature spaces and density estimation methods. The results in Table 5 demonstrate that performing channel-wise density estimation leads to a significant improvement on OOD detection accuracy compared to layer-wise density estimation. We argue that this improvement is due to achieving more accurate density estimation in 1-dimensional space with the channel-wise features. Additionally, we observe that performing KDE on the channel-wise features yields further improvements over using Gaussian for most cases. This is expected since KDE is capable of modelling Gaussian as well as non-Gaussian densities, which leads to more accurate density estimations.

**Computation time:** We compare the proposed method with other methods in terms of computation time. We measure the computation time needed to perform detection on all

OOD datasets in the CIFAR-10 experiments for Baseline, ODIN, and Mahalanobis. We cannot obtain the computation time of G-ODIN since the implementation is not publicly available. We show the mean and standard deviation of the computation times in the plot in Fig. 2. The results demonstrate that the Baseline is the fastest method among all methods as expected since it does only a single forward pass in the networks. The proposed method is the second most efficient method despite the high computational cost of KDE. The main reason for ODIN and Mahalanobis being computationally less efficient than the proposed method is the input pre-processing step. This is a computationally heavy step that our method does not have. Mahalanobis is the slowest method among all since it applies input pre-processing before computing the scores at each layer. Although we do not have the computation time results for G-ODIN, we expect it to be similar to ODIN since it consists of a similar input pre-preprocessing step.

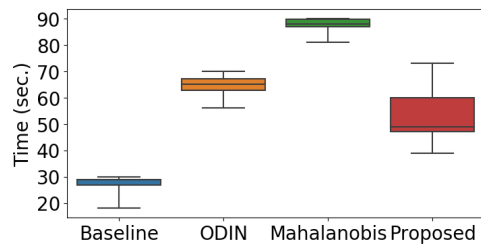


Figure 2: Mean and standard deviation of the computation times of all OOD datasets in the CIFAR-10 experiments.

## 4 Conclusion

In this paper, we presented an unsupervised OOD detection method that learns pdfs of features for each channel of a DNN using KDE. Features of a test image are evaluated at the corresponding pdfs to obtain a confidence score per channel that is expected to be higher for InD images and lower for OOD ones. These scores are combined into a final score using logistic regression classifier, that is pre-trained using InD training images and their adversarially perturbed versions. The use of KDE allows us to learn feature pdfs in a non-parametric manner, and removes the assumption of a particular family of parametric densities. Moreover, the proposed method does not need any image-level class label information and can be applied to both classification and non-classification DNNs, unlike most of the state-of-the-art methods in the literature.

We perform an extensive evaluation on both classification and non-classification networks and compare them with the state-of-the-art methods. In the classification experiments, our method achieves the best OOD detection performance by a significant margin compared to other methods in the majority of the cases. In the non-classification experiments, we perform experiments on both segmentation and detection networks, and our method achieves significant improvement over the existing methods in both these tasks. Finally, we

show that the proposed method is the second most computationally efficient among all compared methods.

## 5 Ethics statement

Deep neural networks have achieved significant advancement to the state-of-the-art in many image analysis tasks ranging from computer vision to medical image analysis. However, their performance may drop significantly if the test image distribution is even slightly different than the training distribution. Moreover, neural networks make predictions on such images with very high confidence. This creates a big obstacle when deploying neural networks for real applications, especially the ones that have a low tolerance for error such as autonomous driving and medical diagnosis. For example, a DNN can diagnose a cancer patient as non-cancer due to a small difference in the setting of MRI scanner and can cause serious problems.

Detecting out-of-distribution images is a crucial step for improving the robustness and reliability of neural networks especially for safety-critical applications. Incorporating an out-of-distribution detector to the neural networks can introduce a safety layer that alerts the user when the networks are likely to make mistakes. Most of the existing methods in the literature focus on detecting out-of-distribution images in classification networks. However, out-of-distribution detection is crucial for other type of neural networks such as segmentation, object detection, and depth estimation as well. Developing out-of-distribution detection methods that can work for both classification and non-classification networks is quite important, but this is explored less compared to the classification networks. In this paper, we take a step towards tackling this issue and propose an out-of-distribution detection method that can work with any type of neural network.

## Acknowledgements

The presented work was partly funding by: 1. Clinical Research Priority Program Grant on Artificial Intelligence in Oncological Imaging Network, University of Zurich, 2. Swiss Data Science Center (DeepMicroIA), 3. Swiss Platform for Advanced Scientific Computing (PASC), coordinated by Swiss National Super-computing Centre (CSCS), 4. Personalized Health and Related Technologies (PHRT), project number 222, ETH domain. We also thank Nvidia for their GPU donation.

## References

Alhaija, H. A.; Mustikovela, S. K.; Mescheder, L.; Geiger, A.; and Rother, C. 2018. Augmented reality meets computer vision: Efficient data generation for urban driving scenes. *International Journal of Computer Vision* 126(9): 961–972.

Amodei, D.; Olah, C.; Steinhardt, J.; Christiano, P.; Schulman, J.; and Mané, D. 2016. Concrete problems in AI safety. *arXiv preprint arXiv:1606.06565*.

Chen, L.-C.; Papandreou, G.; Schroff, F.; and Adam, H. 2017. Rethinking atrous convolution for semantic image segmentation. *arXiv preprint arXiv:1706.05587*.

Davis, J.; and Goadrich, M. 2006. The relationship between Precision-Recall and ROC curves. In *Proceedings of the 23rd international conference on Machine learning*, 233–240. ACM.

Deng, J.; Dong, W.; Socher, R.; Li, L.-J.; Li, K.; and Fei-Fei, L. 2009. Imagenet: A large-scale hierarchical image database. In *2009 IEEE conference on computer vision and pattern recognition*, 248–255. Ieee.

DeVries, T.; and Taylor, G. W. 2018. Learning Confidence for Out-of-Distribution Detection in Neural Networks. *arXiv preprint arXiv:1802.04865*.

Erdil, E.; Yildirim, S.; Tasdizen, T.; and Cetin, M. 2019. Pseudo-Marginal MCMC Sampling for Image Segmentation Using Nonparametric Shape Priors. *IEEE Transactions on Image Processing* 28(11): 5702–5715.

Everingham, M.; Van Gool, L.; Williams, C. K.; Winn, J.; and Zisserman, A. 2010. The pascal visual object classes (voc) challenge. *International journal of computer vision* 88(2): 303–338.

Guo, C.; Pleiss, G.; Sun, Y.; and Weinberger, K. Q. 2017. On calibration of modern neural networks. In *Proceedings of the 34th International Conference on Machine Learning-Volume 70*, 1321–1330. JMLR. org.

He, K.; Zhang, X.; Ren, S.; and Sun, J. 2016. Deep residual learning for image recognition. In *Proceedings of the IEEE conference on computer vision and pattern recognition*, 770–778.

Hendrycks, D.; and Gimpel, K. 2017. A Baseline for Detecting Misclassified and Out-of-Distribution Examples in Neural Networks. *Proceedings of International Conference on Learning Representations*.

Hendrycks, D.; Mazeika, M.; and Dietterich, T. 2018. Deep anomaly detection with outlier exposure. *arXiv preprint arXiv:1812.04606*.

Hendrycks, D.; Mazeika, M.; Kadavath, S.; and Song, D. 2019. Using self-supervised learning can improve model robustness and uncertainty. In *Advances in Neural Information Processing Systems*, 15637–15648.

Hsu, Y.-C.; Shen, Y.; Jin, H.; and Kira, Z. 2020. Generalized odin: Detecting out-of-distribution image without learning from out-of-distribution data. In *Proceedings of the IEEE/CVF Conference on Computer Vision and Pattern Recognition*, 10951–10960.

Krizhevsky, A.; Hinton, G.; et al. 2009. Learning multiple layers of features from tiny images. Technical report, Cite-seer.

Lee, K.; Lee, H.; Lee, K.; and Shin, J. 2018a. Training Confidence-Calibrated Classifiers for Detecting Out-of-Distribution Samples. In *ICLR 2018*. ICLR 2018.

Lee, K.; Lee, K.; Lee, H.; and Shin, J. 2018b. A simple unified framework for detecting out-of-distribution samples and adversarial attacks. In *Advances in Neural Information Processing Systems*, 7167–7177.



- Liang, S.; Li, Y.; and Srikant, R. 2017. Enhancing the reliability of out-of-distribution image detection in neural networks. *arXiv preprint arXiv:1706.02690* .
- Lin, T.-Y.; Maire, M.; Belongie, S.; Hays, J.; Perona, P.; Ramanan, D.; Dollár, P.; and Zitnick, C. L. 2014. Microsoft coco: Common objects in context. In *European conference on computer vision*, 740–755. Springer.
- Nalisnick, E.; Matsukawa, A.; Teh, Y. W.; Gorur, D.; and Lakshminarayanan, B. 2018. Do deep generative models know what they don't know? *arXiv preprint arXiv:1810.09136* .
- Netzer, Y.; Wang, T.; Coates, A.; Bissacco, A.; Wu, B.; and Ng, A. Y. 2011. Reading digits in natural images with unsupervised feature learning .
- Ren, S.; He, K.; Girshick, R.; and Sun, J. 2015. Faster r-cnn: Towards real-time object detection with region proposal networks. In *Advances in neural information processing systems*, 91–99.
- Scott, D. W. 2015. *Multivariate density estimation: theory, practice, and visualization*. John Wiley & Sons.
- Silverman, B. W. 1986. *Density estimation for statistics and data analysis*, volume 26. CRC press.
- Vyas, A.; Jammalamadaka, N.; Zhu, X.; Das, D.; Kaul, B.; and Willke, T. L. 2018. Out-of-distribution detection using an ensemble of self supervised leave-out classifiers. In *Proceedings of the European Conference on Computer Vision (ECCV)*, 550–564.
- Xu, P.; Ehinger, K. A.; Zhang, Y.; Finkelstein, A.; Kulkarini, S. R.; and Xiao, J. 2015. Turkergaze: Crowdsourcing saliency with webcam based eye tracking. *arXiv preprint arXiv:1504.06755* .
- Yu, F.; Chen, H.; Wang, X.; Xian, W.; Chen, Y.; Liu, F.; Madhavan, V.; and Darrell, T. 2020. Bdd100k: A diverse driving dataset for heterogeneous multitask learning. In *The IEEE Conference on Computer Vision and Pattern Recognition (CVPR)*.
- Yu, F.; Seff, A.; Zhang, Y.; Song, S.; Funkhouser, T.; and Xiao, J. 2015. Lsun: Construction of a large-scale image dataset using deep learning with humans in the loop. *arXiv preprint arXiv:1506.03365* .
- Zhou, B.; Lapedriza, A.; Khosla, A.; Oliva, A.; and Torralba, A. 2017. Places: A 10 million image database for scene recognition. *IEEE transactions on pattern analysis and machine intelligence* 40(6): 1452–1464.

## A Experiments on Mask R-CNN trained on COCO

In this section, we present experiments on a new detection network architecture, Mask R-CNN, trained on COCO datasets. We compare our results with SSL and Mahalanobis as shown in Table 6. In this network architecture, the proposed method achieves OOD detection almost without any error while the other methods do not perform well.

OOD	FPR at 95% TPR ↓	AUROC ↑	Detection Error ↓
	SSL / Mahalanobis / <b>Proposed</b>		
Pascal VOC	95.42 / 94.23 / <b>0.0</b>	50.87 / 49.06 / <b>99.70</b>	50.21 / 49.61 / <b>2.50</b>
KITTI	88.81 / 99.29 / <b>0.0</b>	58.29 / 14.75 / <b>99.01</b>	46.90 / 52.14 / <b>2.50</b>
BDD	94.07 / 94.69 / <b>0.0</b>	51.95 / 44.40 / <b>99.64</b>	49.53 / 49.84 / <b>2.50</b>
Places	94.67 / 95.04 / <b>0.0</b>	50.68 / 47.69 / <b>99.75</b>	49.83 / 50.02 / <b>2.50</b>

Table 6: Quantitative results on distinguishing test set of COCO InD dataset from several OOD datasets in the detection network trained on Mask R-CNN architecture.

## B Discussion on generative models-based OOD detection methods

In addition to the OOD detection methods we discussed in the main paper that operate on discriminative neural networks, there is also a line of work that focuses on the OOD detection on generative models. OOD detection accuracy of these methods are not yet on the level of the OOD detection methods designed for discriminative networks. The generative models suffer from diminished OOD detection accuracy since these models assign higher probabilities to the OOD samples than the InD samples (Nalisnick et al. 2018). For the sake of the completeness, we compare our results with a recent generative model-based OOD detection method proposed by Hendryks et al. (2018) in Tables 7 and 8. For comparison, we collected the results from the experiments that are common in our main paper and Hendryks et al. (2018). In these experiments, Hendryks et al. (2018) use PixelCNN++ as generative model on both CIFAR-10 and CIFAR-100 datasets. The results demonstrate that our method significantly outperforms Hendryks et al. (2018) on these experiments.

OOD	FPR at 95% TPR ↓	AUROC ↑
	Hendryks et al. (2018) / Proposed	
SVHN	86.9 / <b>6.8</b>	75.8 / <b>97.8</b>
LSUN	43.2 / <b>1.1</b>	90.9 / <b>99.6</b>

Table 7: Comparison of the proposed method with a generative model-based OOD detection method on CIFAR-10 dataset.

OOD	FPR at 95% TPR ↓	AUROC ↑
	Hendryks et al. (2018) / Proposed	
SVHN	42.9 / <b>4.8</b>	86.9 / <b>98.0</b>
LSUN	57.5 / <b>1.7</b>	83.4 / <b>99.4</b>

Table 8: Comparison of the proposed method with a generative model-based OOD detection method on CIFAR-100 dataset.

## C Analysis with different $N$

$N$  is a hyperparameter of the proposed method that determines number of samples to be used for unbiased estimation of the target density using KDE. In this section, we analyze the behavior of the proposed approach as a function of different  $N$  values. We present the OOD detection performance using different metrics for both CIFAR-10 and CIFAR-100 experiments in Tables 9 and 10, respectively.

## D AUROC trends for CIFAR-100 datasets

In the main paper, we demonstrate that the similarities between channel-wise AUROC trends of adversarial examples and the OOD datasets play a significant role on OOD detection accuracy for CIFAR-10 dataset. We conduct the same analysis for the CIFAR-100 dataset to demonstrate that this observation holds for various datasets. We plot the trends for the OOD datasets and the adversarial examples for the network trained on CIFAR-100 dataset in Fig. 3. SVHN, TIN-rs, LSUN-rs, and iSUN have very similar trends with the adversarial images which explains the better performance on these OOD datasets.

OOD	FPR at 95% TPR ↓	AUROC ↑	Detection Error ↓
		$N = 1000/2000/5000/7000$	
SVHN	24.58 / 14.90 / 6.80 / 7.00	92.84 / 95.91 / 97.87 / 97.99	14.79 / 9.95 / 5.90 / 6.00
TIN-rs	1.39 / 1.31 / 1.91 / 2.33	99.15 / 99.28 / 99.05 / 99.20	3.19 / 3.15 / 3.45 / 3.66
TIN-cr	75.03 / 76.60 / 72.01 / 71.41	78.47 / 78.07 / 78.88 / 79.40	40.01 / 40.80 / 38.50 / 38.20
LSUN-rs	0.49 / 0.56 / 1.12 / 1.41	99.72 / 99.73 / 99.62 / 99.60	2.74 / 2.78 / 3.06 / 3.20
LSUN-cr	80.63 / 78.35 / 79.79 / 80.67	69.83 / 71.94 / 71.63 / 70.30	42.81 / 41.67 / 42.39 / 42.83
iSUN	1.38 / 1.26 / 2.06 / 2.48	99.17 / 99.24 / 98.93 / 99.05	3.19 / 3.13 / 3.53 / 3.74

Table 9: Performance of the proposed method on CIFAR-10 dataset as a function of number of samples ( $N$ ) that are used in KDE.

OOD	FPR at 95% TPR ↓	AUROC ↑	Detection Error ↓
		$N = 1000/2000/5000/7000$	
SVHN	8.61 / 8.71 / 4.87 / 4.67	95.75 / 97.15 / 98.05 / 98.49	6.80 / 6.85 / 4.93 / 4.83
TIN-rs	6.31 / 4.87 / 6.16 / 9.11	98.16 / 98.63 / 98.18 / 98.12	5.65 / 4.93 / 5.58 / 7.05
TIN-cr	80.44 / 78.52 / 78.15 / 75.87	74.68 / 72.68 / 75.01 / 75.70	42.72 / 41.76 / 41.57 / 40.43
LSUN-rs	4.03 / 1.20 / 1.70 / 2.51	98.69 / 99.51 / 99.41 / 99.27	4.51 / 3.10 / 3.35 / 3.75
LSUN-cr	76.11 / 66.82 / 65.22 / 61.62	71.96 / 80.33 / 81.54 / 82.68	40.55 / 35.91 / 35.11 / 33.31
iSUN	5.32 / 4.28 / 4.41 / 7.68	98.45 / 99.15 / 98.91 / 98.65	5.16 / 4.64 / 4.70 / 6.34

Table 10: Performance of the proposed method on CIFAR-100 dataset as a function of number of samples ( $N$ ) that are used in KDE.

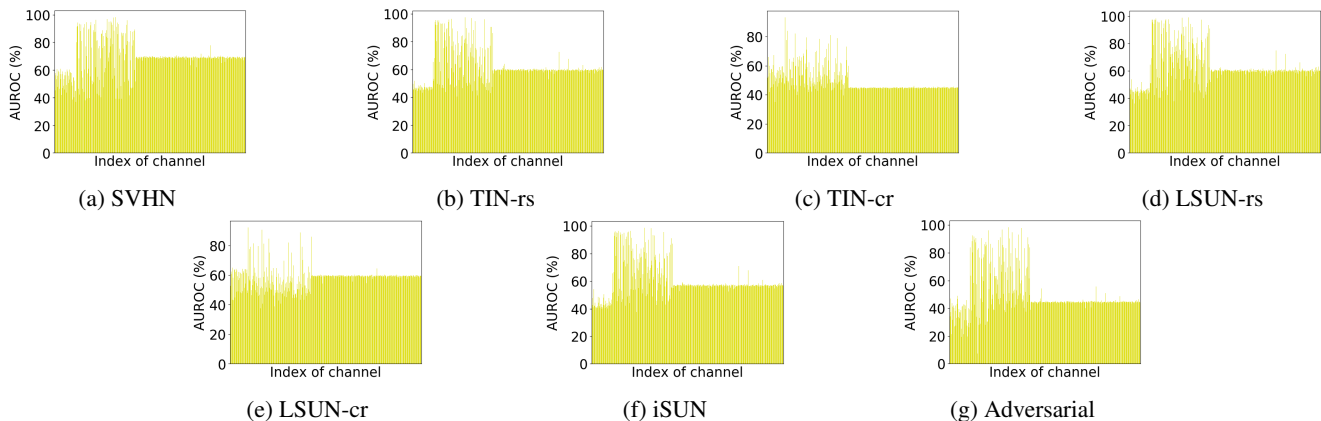


Figure 3: Trends of channel-wise OOD detection performance evaluated with AUROC for different OOD datasets when the InD dataset is CIFAR-100. The plots show that the AUROC trend of adversarial images is similar to most of the OOD datasets, indicating that the logistic regression classifier trained using adversarial images can generalize to most of the OOD datasets.